Available online at www.sciencedirect.com
ScienceDirect
J. Vis. Commun. Image R. 18 (2007) 331–340
JOURNAL OF VISUAL Communication & IMAGE Representation
www.elsevier.com/locate/jvci

Efficient hybrid error concealment algorithm based on adaptive estimation scheme ☆

Kuo-Liang Chung [a,*], Tzu-Huang Huang [b], Po-Hsuan Liao [a]

[a] *Department of Computer Science and Information Engineering, National Taiwan University of Science and Technology, No. 43, Section 4, Keelung Road, Taipei 10672, Taiwan, ROC*

[b] *Institute of Automation and Control, National Taiwan University of Science and Technology, No. 43, Section 4, Keelung Road, Taipei 10672, Taiwan, ROC*

Received 14 June 2006; accepted 27 April 2007
Available online 10 May 2007

Abstract

Video transmission plays an important role in multimedia communication. Due to transmission error; robust video transmission has become increasingly important in providing better quality of services. Based on our proposed novel adaptive estimation scheme, this paper presents an efficient hybrid error concealment algorithm for robust video transmission. Using the information of neighboring macroblocks (MBs) of the corrupted MBs, the corrupted MBs are first classified into three types. According to the type of the corrupted MB, our proposed adaptive estimation scheme could adopt the Bézier surface estimation, the first-order plane estimation, or the centroid of major cluster estimation to conceal the corrupted MB efficiently. Based on six testing video sequences, experimental results demonstrate that our proposed hybrid error concealment algorithm can improve the video quality and the execution-time performance over different loss rates.

Keywords: Bézier surface; Centroid; Cluster; Error concealment; First-order plane; Motion vector

1. Introduction

Most video sequence coding systems use the block motion compensation to remove temporal redundancy for video compression. In real world, due to the transmission error, the video sequence coding systems cannot provide a completely guaranteed quality of services. Thus, error concealment for corrupted macroblocks (MBs) is necessary in decoding phase to increase the transmission quality. In this research, we assume that the corrupted MBs in the current frame are known in advance. The readers are suggested to refer to the previous efficient algorithms [4,11,14,22] for detecting the damaged MBs. In the past years, based on this assumption, many error concealment algorithms have been developed. These developed error concealment approaches can be classified into three types, namely the temporal error concealment, the spatial error concealment, and the temporal- and spatial-based error concealment.

Among these temporal-based error concealment algorithms, the corrupted MB can be estimated by using the information of the neighboring regions of the reference MB with the same location of the corrupted MB; the best matching MB in the search region of the previous frame is used to replace the corrupted MB. Al-Mualla et al. [1] presented a temporal error concealment algorithm using two techniques, the bilinear motion field interpolation and the boundary matching scheme. Zhang et al. [19] presented an efficient motion vector-based algorithm to estimate the corrupted MBs. In order to reduce the error propagation to the succeeding frames, Lee et al. [12] presented a multi-frame boundary matching algorithm which utilizes the boundary smoothness property in the decoded

☆ Supported by National Science Council of ROC under contracts NSC94-2213-E-011-041 and NSC95-2221-E-011-152.
* Corresponding author. Fax: +886 2 273 76777.
E-mail address: k.l.chung@mail.ntust.edu.tw (K.-L. Chung).

1047-3203/$ - see front matter © 2007 Elsevier Inc. All rights reserved.
doi:10.1016/j.jvcir.2007.04.007

and succeeding frames. Feng et al. [5] presented a modified boundary matching algorithm to determine the best matching block in the reference frame for recovering the corrupted MB. Based on the motion estimation of enlarged block, Jang and Ra [8] presented an efficient error localization and temporal error concealment algorithm. Using the concept of block-wise similarity within a frame, Wang et al. [17] presented a best neighborhood matching algorithm for error concealment. Among these spatial-based error concealment algorithms, the damaged MB is recovered by using the spatial information within the current frame. Park and Lee [13] utilized a non-uniform rational B-spline approximation to estimate the damaged MB. Zhao et al. [20] presented a spatial error concealment approach based on the directional decision and the intra-prediction. Zeng and Liu [18] presented a directional filtering scheme which uses the extracted geometric information to preserve the geometric structure of the corrupted MB. Among these developed temporal- and spatial-based error concealment algorithms, both temporal and spatial information are used to estimate the corrupted MB. Kang and Leou [10] concealed the lost MB occurred in the intra-frames and inter-frames by using the spatial linear interpolation and the boundary matching technique. Combining the side-match criterion [9] and the overlapped motion compensation, Chen et al. [2] presented an efficient error concealment algorithm. Tsekeridou et al. [16] presented a block-matching principle which consists of the split-match and the forward–backward block-match techniques. Recently, Chen et al. [3] presented a more efficient error concealment algorithm using the recursive block-matching principle. Zheng and Chau [21] presented an efficient first-order plane estimation to conceal the corrupted MB for the video coding standard H.26 L [15]. In their error concealment method, the motion vectors of four neighboring of the corrupted MB are used to estimate the four corners of the corrupted MB. Although a 16×16 MB in H.26 L can be divided into different block division modes, their method can be applied to the other video coding systems. The simulation results demonstrate that the first-order plane estimation outperforms the temporal replacement method.

Based on our proposed novel adaptive estimation scheme, this paper presents a hybrid error concealment algorithm for robust video transmission. Based on the eight neighboring MBs of the corrupted MBs, the corrupted MBs can be classified into three types, the tie and high variance type (TAH), the tie and low variance (TAL) type, and the dominance type. According to the classified type of the current corrupted MB, our proposed hybrid error concealment (HEC) algorithm can determine what kind of error concealment method should be used to recover the damaged MB. If the corrupted MB belongs to the TAH (TAL) type, the proposed Bézier surface (the existing first-order plane) estimation is used to conceal the corrupted MB. The reason to explain why the Bézier surface estimation is better than the first-order plane estimation for the TAH type and why using centroid instead of first-order plane estimation for the dominance type will be described in Section 3. If the corrupted MB belongs to the dominance type, the centroid of major cluster estimation is used to conceal the corrupted MB. Experimental results demonstrate that our proposed algorithm can efficiently improve the video quality and the execution-time performance over different MB loss rates when compared to the currently published error concealment algorithm by Zheng and Chau [21].

The remainder of this paper is organized as follows. Section 2 surveys the previous first-order plane estimation for error concealment by Zheng and Chau. Section 3 presents our proposed hybrid error concealment algorithm. Experimental results are demonstrated in Section 4. Conclusions are addressed in Section 5.

2. The past work by Zheng and Chau

In this section, the currently published error concealment algorithm by Zheng and Chau is surveyed. Their algorithm is based on the first-order plane estimation. In Zheng and Chau's result, for one 16×16 MB, there are seven different block division modes to fit the requirement of H.26 L [15]. We only consider the case for mode 0, i.e. the 16×16 MB, to introduce the first-order plane estimation. In fact, the concept of plane equations and bilinear interpolation technique used in the first-order plane estimation can be easily applied to the remaining six different block division modes for error concealment.

The corrupted MB and its eight neighboring MBs are shown in Fig. 1a where $MB_{i,j}$ denotes the corrupted MB and the set $NB = \{MB_{i-1,j-1}, MB_{i,j-1}, MB_{i+1,j-1}, MB_{i-1,j}, MB_{i+1,j}, MB_{i-1,j+1}, MB_{i,j+1}, MB_{i+1,j+1}\}$ denotes the eight neighboring MBs of $MB_{i,j}$. In Fig. 1b, the eight motion vectors of the set NB are denoted by $MV_{i-1,j-1}$, $MV_{i,j-1}$,..., and $MV_{i+1,j+1}$. The motion vector of $MB_{i,j}$, $MV_{i,j}$, is estimated by two-phase approach. In the first phase, the motion vectors of the four corners of the corrupted MB, $MV^1_{i,j}$, $MV^2_{i,j}$, $MV^3_{i,j}$, and $MV^4_{i,j}$, are estimated by using the first-order plane estimation. For simplicity, we only introduce how to estimate the left-top motion

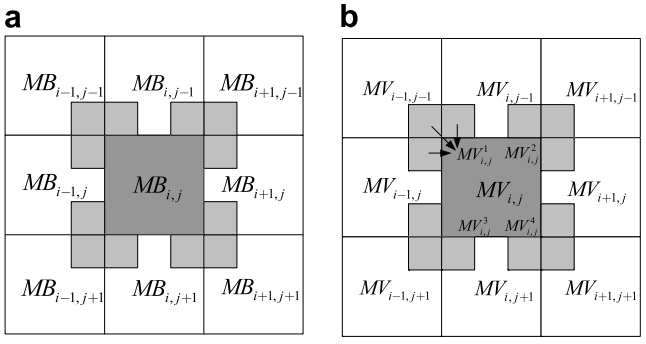

Fig. 1. The depiction of first-order plane estimation. (a) The corrupted MB and its eight neighboring MBs. (b) The estimation of left-top motion vector for corrupted MB.

vector of $MB_{i,j}$, i.e. $MV^1_{i,j}$ (see Fig. 1b). For this case, the known motion vectors $MV_{i-1,j}$, $MV_{i-1,j-1}$, and $MV_{i,j-1}$ are used to estimate $MV^1_{i,j}$ by using the first-order plane.

As shown in Fig. 2, assume that in the current frame, the coordinate of the top-left pixel in the corrupted MB is $(0,0)$ and the coordinates of three central pixels in $MB_{i-1,j}$, $MB_{i-1,j-1}$, and $MB_{i,j-1}$ are $(-2.5,-1.5)$, $(-2.5,2.5)$, and $(1.5,2.5)$, respectively. Considering the three motion vectors of $MB_{i-1,j}$, $MB_{i-1,j-1}$, and $MB_{i,j-1}$ as the values in Z-axis of the 3-D space, the coordinates of the three central pixels are thus denoted by $(-2.5,-1.5,MV_{i-1,j})$, $(-2.5,2.5,MV_{i-1,j-1})$, and $(1.5,2.5,MV_{i,j-1})$, respectively. Based on the new coordinates of the three central pixels, the first-order plane P can be constructed by the following plane equation:

$$\frac{x}{a}+\frac{y}{b}+\frac{z}{c}=1 \tag{1}$$

where

$$a=\frac{2.5MV_{i-1,j}-MV_{i-1,j-1}+2.5MV_{i,j-1}}{MV_{i-1,j-1}-MV_{i,j-1}}$$
$$b=\frac{2.5MV_{i-1,j}-MV_{i-1,j-1}+2.5MV_{i,j-1}}{MV_{i-1,j}-MV_{i-1,j-1}}$$
$$c=\frac{2.5MV_{i-1,j}-MV_{i-1,j-1}+2.5MV_{i,j-1}}{4}$$

Because the coordinate of the left-top motion vector of $MB_{i,j}$ is defined to $(0,0)$, by Eq. (1), $c=\frac{2.5MV_{i-1,j}-MV_{i-1,j-1}+2.5MV_{i,j-1}}{4}$ can be used to estimate $MV^1_{i,j}$. $MV^2_{i,j}$, $MV^3_{i,j}$ and $MV^4_{i,j}$ can also be estimated in a similar way.

After estimating the four motion vectors at four corners of the corrupted MB, in the second phase, a bilinear interpolation is applied to estimate the motion vector of each pixel in the corrupted MB. Given the coordinate of each pixel in the corrupted MB, the motion vector of that pixel located at (x,y) can be estimated by the following bilinear interpolation:

$$MV_{\widetilde{x},\widetilde{y}}=MV^1_{i,j}[\widetilde{y}(1-\widetilde{x})]+MV^2_{i,j}(\widetilde{x}\widetilde{y})+MV^3_{i,j}[(1-\widetilde{x})(1-\widetilde{y})]+MV^4_{i,j}[\widetilde{x}(1-\widetilde{y})] \tag{2}$$

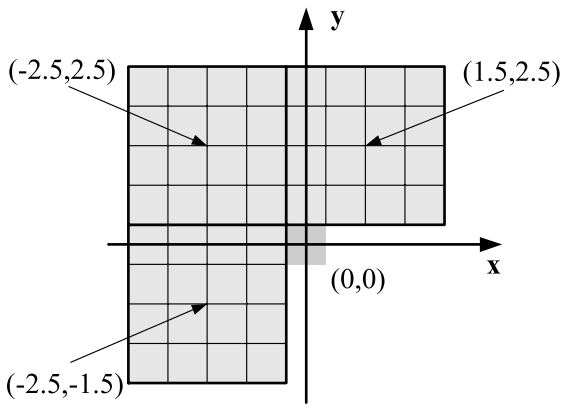

Fig. 2. The coordinates of three central pixels of neighboring MBs.

where $\widetilde{x}$ and $\widetilde{y}$ represent the normalized pixel coordinates that are calculated by $\widetilde{x}=\frac{x-x_0}{x_1-x_0}$ and $\widetilde{y}=\frac{y-y_0}{y_1-y_0}$; x_0, x_1, y_0, and y_1 represent the boundary coordinates of lost MB in the left, right, bottom, and top sides, respectively.

In summary, the first-order plane estimation proposed by Zheng and Chau uses four plane equations (see Eq. (1)) to compute the motion vectors of the four corners of the corrupted MB and then Eq. (2) is used to conceal each pixel of the corrupted MB.

3. Our proposed hybrid error concealment algorithm

In first section, we describe how to classify the corrupted MBs into three types. We then describe what kind of error concealment method among the three feasible methods should be used when the type of the corrupted MB is determined. In second subsection, our proposed Bézier surface estimation method, which is one of the three used estimation methods in the proposed HEC algorithm, is presented. In last subsection, our proposed HEC algorithm is presented.

3.1. Classifying corrupted MBs into three types

For each corrupted MB, $MB_{i,j}$, according to the motion vectors of eight neighboring MBs of $MB_{i,j}$, i.e. NB, we first apply the K-means ($K=2$) clustering method to partition the NB into two clusters. According to eight motion vectors of NB, suppose these eight motion vectors have been partitioned into two clusters, C_1 and C_2, by using the K-means clustering method. We further compute two variances of the eight motion vectors of NB for x axis and y axis; let the two obtained variances be denoted by σ_x^2 and σ_y^2, respectively. Based on $|C_1|$, $|C_2|$, σ_x^2, and σ_y^2, the corrupted MBs can be classified into three types, the tie and high variance (TAH) type, the tie and low variance (TAL) type, and the dominance type. For a corrupted MB, its type can be used to determine the most suitable one among the three error concealment methods.

Definition 1. (Corrupted MB being TAH type) When $\||C_1|-|C_2|\|\leqslant 2$ and $\sigma_x^2>T_v$ (or $\sigma_y^2>T_v$), the corrupted MB is of TAH type where T_v is a specified threshold. Here, we set $T_v=6$ which is explained in the following paragraph.

As shown in Fig. 3a, using the K-means clustering method, the eight neighboring MBs are partitioned into two clusters, C_1 and C_2, where C_1 is denoted by four white MBs and C_2 is denoted by four gray MBs. Considering the condition $\||C_1|-|C_2|\|\leqslant 2$ in Definition 1, we assume $|C_1|\geqslant|C_2|$ for convenience. The pair $(|C_1|,|C_2|)$ satisfying this condition may be $(5,3)$ or $(4,4)$. For the pair $(5,3)$ or the pair $(4,4)$, it reveals that may be the cluster C_1 belongs to one region and the cluster C_2 belongs to the adjacent region. On the other hand, for the condition $\||C_1|-|C_2|\|\leqslant 2$, the corrupted MB is located at the boundary of the two adjacent regions. We further examine the two variances,

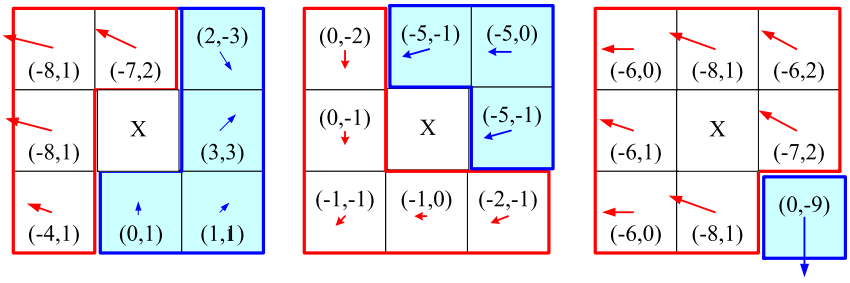

(a) TAH type. (b) TAL type. (c) Dominance type.

Fig. 3. Examples of three classified types of corrupted MBs.

σ_x^2 and σ_y^2, along the x axis and the y axis, respectively, in order to know the variation degree of the surface covering the cluster C_1 and the cluster C_2. Considering the x (y) coordinate of each motion vector among the eight neighboring motion vectors, since the search window is of size 33×33, the motion displacement is ranged from 0 to 16 along the x (y) axis. Here, we set the average motion displacement 8 ($= \frac{0+16}{2}$) to be the upper bound of the threshold T_v and set the square root of the maximal motion displacement, 4 ($= \sqrt{16}$), to be the lower bound of T_v. Empirically, we set the average bound 6 (=(4 + 8)/2) to be the variance threshold T_v. Return to Fig. 3a again. According to the motion vectors of the eight neighboring MBs, we have two variances $\sigma_x^2 = 19.38$ and $\sigma_y^2 = 3.38$. By Definition 1, because of $\|C_1| - |C_2\| \leqslant 2$ and $\sigma_x^2 (= 19.38) > T_v (= 6)$, the type of the corrupted MB as shown in Fig. 3a belongs to the TAH type.

When the corrupted MB belongs to the TAH type, by Definition 1, the corrupted MB is highly possible on a surface with high variation, where the surface contains the clusters C_1 and C_2. For the corrupted MB being TAH type, since the concerned surface is of high variation, we adopt the Bézier surface fitting technique used in computer graphics [7] to emulate the surface which can be constructed by our proposed method described in Section 3.2. Based on the constructed Bézier surface, the lost motion vector of the corrupted MB can be estimated efficiently. For the corrupted MB being TAH type, our proposed Bézier surface estimation for error concealment will be described in next section.

Definition 2. (Corrupted MB being TAL type) When $\|C_1| - |C_2\| \leqslant 2$, $\sigma_x^2 \leqslant T_v$, and $\sigma_y^2 \leqslant T_v$, the corrupted MB is of TAL type where $T_v = 6$ is a specified threshold.

As shown in Fig. 3b, by using the K-means clustering method, the eight neighboring MBs are partitioned into two clusters, C_1 and C_2, where C_1 is denoted by five white MBs and C_2 is denoted by three gray MBs. According to the motion vectors of eight neighboring MBs, we have two variances $\sigma_x^2 = 4.63$ and $\sigma_y^2 = 1.13$. By Definition 2, because of $\|C_1| - |C_2\| \leqslant 2$, $\sigma_x^2 (= 4.63) < T_v (= 6)$, and σ_y^2 $(=1.13) < T_v (=6)$, the type of the corrupted MB as shown in Fig. 3b belongs to the TAL type. The discussion for the condition $\|C_1| - |C_2\| \leqslant 2$ reveals that the corrupted MB is located at the boundary of the two adjacent regions. From $\sigma_x^2 < T_v$ and $\sigma_y^2 < T_v$, we know that along the x axis and the y axis, the variation degree of the surface covering the cluster C_1 and the cluster C_2 is low.

When the corrupted MB belongs to the TAL type, by Definition 2, the corrupted MB is highly possible on a surface with low variation, where the surface contains the clusters C_1 and C_2. For the corrupted MB being TAL type, since the concerned surface is of low variation, we adopt the polygonal mesh model [6] to emulate this kind of surface. In [6], plane equations (see Eq. (1)) are good mathematical model to emulate it. From the description for the first-order plane estimation (see Section 2), Zheng and Chau [21] utilized four plane equations to estimate four corner motion vectors of the corrupted MB, and then utilized bilinear interpolation to conceal the lost motion vectors of all pixels in the corrupted MB. Consequently, we adopt the first-order plane estimation technique to handle the corrupted MB being TAL type.

Definition 3. (Corrupted MB being dominance type) When $\|C_1| - |C_2\| \geqslant 4$, the corrupted MB is of dominance type.

As shown in Fig. 3c, by using the K-means clustering method, the eight neighboring MBs are partitioned into two clusters, C_1 and C_2; one is denoted by seven white MBs and another one is denoted by one gray MBs. By Definition 3, because of $\|C_1| - |C_2\| \geqslant 4$, the type of the corrupted MB as shown in Fig. 3c belongs to the dominance type. For exposition, we still suppose $|C_1| > |C_2|$. When a corrupted MB is of dominance type, the pair $(|C_1|, |C_2|)$ may be $(8,0)$, $(7,1)$, or $(6,2)$. For the case $(|C_1|, |C_2|) = (8,0)$ and $(|C_1|, |C_2|) = (7,1)$, the corrupted MB is inside the major cluster C_1; for the case $(|C_1|, |C_2|) = (6,2)$, it is highly possible that the corrupted MB is a portion of the major cluster C_1. From the above analysis, for dominance type, the corrupted MB can be concealed by using the information of motion vectors in the major cluster C_1, and we ignore the motion vectors in the smaller cluster C_2 due to $|C_1| - |C_2| \geqslant 4$. Consequently, when the corrupted MB is of dominance type, for saving execution time requirement, it is a feasible way to estimate the lost motion vectors of the corrupted MB by using the centroid of major cluster C_1. That is, according to the

centroid of major cluster, we get the corresponding MB in the reference frame, and use it to replace the corrupted MB.

3.2. Bézier surface estimation

In this section, our proposed Bézier surface estimation is presented to conceal the corrupted MB being the TAH type. The Bézier surface is represented as the cartesian product of the blending functions of two orthogonal Bézier curves [7] and that surface $B(u,v)$ is expressed by

$$B(u,v)=\sum_{i=0}^{m}\sum_{j=0}^{n}P_{i,j}C(m,i)u^i(1-u)^{m-i}C(n,j)v^j(1-v)^{n-j},\quad 0\leqslant u\leqslant 1, 0\leqslant v\leqslant 1, \tag{3}$$

where $C(m,i)=\frac{m!}{i!(m-i)!}$ and $C(n,j)=\frac{n!}{j!(n-j)!}$; $P_{i,j}$ is the i, jth control point. Eq. (3) reveals that there are $(m+1)\times(n+1)$ control points in the 3-D space. Fig. 4 illustrates the Bézier surface with nine control points for $m=2$ and $n=2$; the control points are connected by dashed lines, and the solid lines constitute the patches of the Bézier surface. The corresponding point for $u=v=0$ on the Bézier surface is the control point $P_{1,1}$; for $u=v=1$, the corresponding point is the control point $P_{3,3}$.

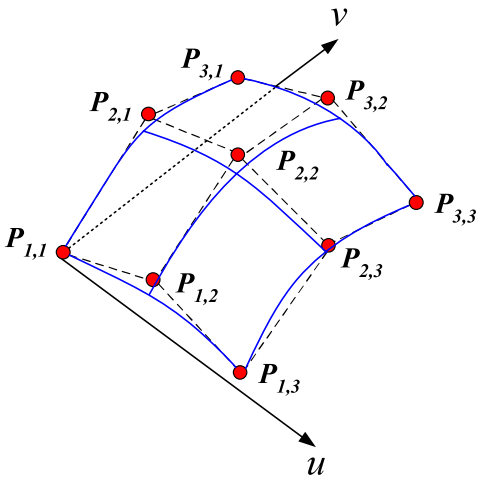

Fig. 4. One Bézier surface constructed by nine control points for $m=2$ and $n=2$.

Based on the Bézier surface estimation, our proposed error concealment method is now presented when the corrupted MB is of TAH type. As mentioned before, the location of the corrupted MB has been detected and its own eight neighboring MBs have been decoded successfully. As shown in Fig. 5a, the control point $P_{2,2}(u=\frac{1}{2},v=\frac{1}{2})$ denotes the location of the corrupted MB and the set of control points $CP=\{P_{1,1}(0,0),P_{2,1}(\frac{1}{2},0),P_{3,1}(1,0),P_{1,2}(0,\frac{1}{2}),P_{3,2}(1,\frac{1}{2}),P_{1,3}(0,1),P_{2,3}(\frac{1}{2},1),P_{3,3}(1,1)\}$ denotes the locations of the eight neighboring MBs. We next map the nine control points in Fig. 5a to the nine motion vectors in Fig. 5b. In Fig. 5b, the nine motion vectors can determine the configuration of the Bézier surface.

After plugging the nine motion vectors into the nine control points, Eq. (3) can be represented by the following form:

$$B(u,v)=[(1-u)^2\ 2u(1-u)\ u^2)]\times[P]\times\begin{bmatrix}(1-v)^2\\2v(1-v)\\v^2\end{bmatrix} \tag{4}$$

where

$$[P]=\begin{bmatrix}\mathrm{MV}_{i-1,j-1} & \mathrm{MV}_{i,j-1} & \mathrm{MV}_{i+1,j-1}\\ \mathrm{MV}_{i-1,j} & \mathrm{MV}_{i,j} & \mathrm{MV}_{i+1,j}\\ \mathrm{MV}_{i-1,j+1} & \mathrm{MV}_{i,j+1} & \mathrm{MV}_{i+1,j+1}\end{bmatrix}.$$

It is known that the location of the corrupted MB is denoted by $P_{2,2}(u=\frac{1}{2},v=\frac{1}{2})$. As a result, the estimated motion vector of the corrupted MB is given by

$$\begin{bmatrix}\frac{1}{4} & \frac{1}{2} & \frac{1}{4}\end{bmatrix}\times[P]\times\begin{bmatrix}\frac{1}{4}\\\frac{1}{2}\\\frac{1}{4}\end{bmatrix}.$$

We thus have

$$\begin{aligned}B\left(\tfrac{1}{2},\tfrac{1}{2}\right)&=\mathrm{MV}_{i,j}\\&=\tfrac{1}{16}\mathrm{MV}_{i-1,j-1}+\tfrac{1}{8}\mathrm{MV}_{i,j-1}+\tfrac{1}{16}\mathrm{MV}_{i+1,j-1}\\&\quad+\tfrac{1}{8}\mathrm{MV}_{i-1,j}+\tfrac{1}{4}\mathrm{MV}_{i,j}+\tfrac{1}{8}\mathrm{MV}_{i+1,j}\\&\quad+\tfrac{1}{16}\mathrm{MV}_{i-1,j+1}+\tfrac{1}{8}\mathrm{MV}_{i,j+1}+\tfrac{1}{16}\mathrm{MV}_{i+1,j+1}.\end{aligned}$$

Equivalently, we have

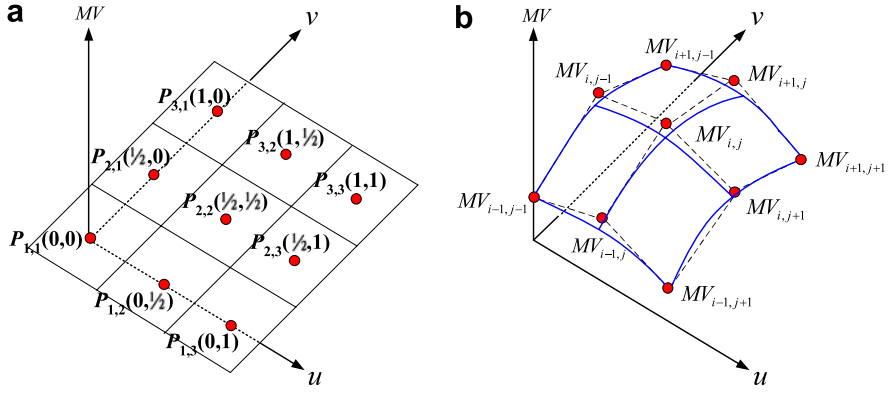

Fig. 5. Using nine motion vectors to construct the Bézier surface. (a) The nine control points of the MBs. (b) The constructed Bézier surface.

$$\begin{aligned}\mathrm{MV}_{i,j} - \tfrac{1}{4}\mathrm{MV}_{i,j} &= \tfrac{1}{16}\mathrm{MV}_{i-1,j-1} + \tfrac{1}{8}\mathrm{MV}_{i,j-1} + \tfrac{1}{16}\mathrm{MV}_{i+1,j-1} \\ &\quad + \tfrac{1}{8}\mathrm{MV}_{i-1,j} + \tfrac{1}{8}\mathrm{MV}_{i+1,j} \\ &\quad + \tfrac{1}{16}\mathrm{MV}_{i-1,j+1} + \tfrac{1}{8}\mathrm{MV}_{i,j+1} + \tfrac{1}{16}\mathrm{MV}_{i+1,j+1}.\end{aligned}$$

Consequently, the estimated motion vector of the corrupted MB can be calculated by

$$\begin{aligned}\mathrm{MV}_{i,j} &= \tfrac{4}{3}\big(\tfrac{1}{16}\mathrm{MV}_{i-1,j-1} + \tfrac{1}{8}\mathrm{MV}_{i,j-1} + \tfrac{1}{16}\mathrm{MV}_{i+1,j-1} \\ &\quad + \tfrac{1}{8}\mathrm{MV}_{i-1,j} + \tfrac{1}{8}\mathrm{MV}_{i+1,j} \\ &\quad + \tfrac{1}{16}\mathrm{MV}_{i-1,j+1} + \tfrac{1}{8}\mathrm{MV}_{i,j+1} + \tfrac{1}{16}\mathrm{MV}_{i+1,j+1}\big) \\ &= \tfrac{1}{12}\mathrm{MV}_{i-1,j-1} + \tfrac{1}{6}\mathrm{MV}_{i,j-1} + \tfrac{1}{12}\mathrm{MV}_{i+1,j-1} \\ &\quad + \tfrac{1}{6}\mathrm{MV}_{i-1,j} + \tfrac{1}{6}\mathrm{MV}_{i+1,j} \\ &\quad + \tfrac{1}{12}\mathrm{MV}_{i-1,j+1} + \tfrac{1}{6}\mathrm{MV}_{i,j+1} + \tfrac{1}{12}\mathrm{MV}_{i+1,j+1}.\end{aligned}$$

Fig. 6 depicts the corresponding 3×3 mask and the estimated motion vector $\mathrm{MV}_{i,j}$ equals to the response when applying the depicted 3×3 mask on the eight motion vectors of neighboring MBs.

3.3. The proposed HEC algorithm

In this section, our proposed HEC algorithm for error concealment is presented. Based on the motion vectors of eight neighboring MBs of the corrupted MB, by using the *K*-means algorithm, the corrupted MB can be determined to one of the three types, the TAH type, the TAL type, or the dominance type. According to the classified type of the damaged MB, our proposed HEC algorithm can determine what kind of the error concealment method should be used. If the corrupted MB belongs to the TAH (TAL) type, the Bézier surface (the first-order plane) estimation is used to conceal the corrupted MB. If the corrupted MB belongs to the dominance type, the centroid of major cluster is used to conceal the corrupted MB. Our proposed HEC algorithm consists of the following eight steps:

Step 1. For the corrupted MB in current image frame, the motion vectors of eight neighboring decoded MBs are given.

$\frac{1}{12}$	$\frac{1}{6}$	$\frac{1}{12}$
$\frac{1}{6}$	X	$\frac{1}{6}$
$\frac{1}{12}$	$\frac{1}{6}$	$\frac{1}{12}$

Fig. 6. The 3×3 mask used to estimate the motion vector of corrupted MB.

Step 2. For the corrupted MB, $\mathrm{MB}_{i,j}$, applying the *K*-means ($K = 2$) clustering method to partition the eight neighboring MBs of $\mathrm{MB}_{i,j}$, say NB, into two clusters, C_1 and C_2. If $\|C_1| - |C_2\| > 2$, go to Step 3; otherwise, go to Step 4.

Step 3. The type of the corrupted MB is the dominance type and use the centroid of the major cluster to estimate the motion vector of the corrupted MB. Go to Step 7.

Step 4. Compute the variances of the eight motion vectors of NB for x axis and y axis; let the two obtained variances be denoted by σ_x^2 and σ_y^2, respectively. If $\sigma_x^2 > T_v$ (or $\sigma_y^2 > T_v$), where $T_v = 6$ is a specified threshold, go to Step 5; otherwise, go to Step 6.

Step 5. The corrupted MB is of TAH type. The Bézier surface estimation is used to estimate the motion vector of the corrupted MB. Go to Step 7.

Step 6. The corrupted MB is of TAL type. The first-order plane estimation is used to estimate the motion vector of the corrupted MB. Go to Step 7.

Step 7. According to the estimated motion vector of the corrupted MB, we can get the corresponding MB in the reference frame, and use it to replace the corrupted MB.

Step 8. Repeat Steps 1–7 until all corrupted MBs have been concealed.

After presenting our proposed whole HEC algorithm, the flowchart for the first seven steps in the proposed algorithm for error concealment is depicted in Fig. 7.

4. Experimental results

In this section, some experiments are demonstrated to show better image quality and execution-time performance of our proposed HEC algorithm when compared to the previous first-order plane estimation algorithm [21]. Six testing video sequences, two 352×288 CIF video sequences (Foreman and Stefan) and four 352×240 SIF video sequences (Salesman, Akiyo, Mobile and Calendar, and Football), are used to evaluate the performance comparison. Since each MB is of size 16×16, there are 396 MBs for each image frame in the CIF video sequences and 330 MBs for each image frame in the SIF video sequences.

The PSNR (Peak Signal-to-Noise Ratio) measure is used to evaluate the image quality in the first-order plane estimation algorithm [21] and our proposed HEC algorithm for different loss rates. Here, the PSNR is defined by

$$\mathrm{PSNR} = 10 \log_{10} \frac{255^2}{\mathrm{MSE}}$$

$$\mathrm{MSE} = \frac{1}{M * N} \sum_{x=0}^{M-1} \sum_{y=0}^{N-1} [I(x,y) - I'(x,y)]^2$$

where $M \times N$ denotes the image size; $I(x,y)$ and $I'(x,y)$ denote the original image frame and the reconstructed image frame. In our experiments, the two loss rates of corrupted

MBs are given by 5% and 10%; the locations of corrupted MBs are randomly specified in advance. The loss rate 5% (10%) means that the number of corrupted MBs over all the MBs in the compensated image is 5% (10%). As shown in Fig. 8a and Fig. 9a, the compensated images are the decompressed *P* frames which are encoded by using the motion estimation technique and the JPEG compression method. Here, the compensated images are also called the error-free images because they are not corrupted. Fig. 8b and Fig. 9b denote the corrupted image frames with loss rates 5% and 10%, respectively, where the corrupted MBs are denoted by black boxes in the compensated image.

In Tables 1 and 2, the term $PSNR_{EF}$ denotes the average PSNR of compensated frames for each of the six testing error-free video sequences. In Tables 1 and 2, under 5% and 10% loss rates, respectively, the term $PSNR_{FOP}$ denotes the average PSNR for each of the six video sequences concealed by he first-order plane estimation. The term $PSNR_{HEC}$ denotes the average PSNR for each of the six video sequences concealed by our proposed HEC algorithm. From the two tables, under 5% and 10% loss rates, the average PSNRs of the error-free algorithm, the previous first-order plane estimation algorithm, and our proposed HEC algorithm are 32.25, 31.72 (=(31.88 + 31.55)/2), and 31.99 (=(32.07 + 31.9)/2), respectively, where the PSNR of the error-free algorithm is equal to the PSNR of the original image over the compensated image without any corrupted MBs. In average, our proposed HEC algorithm has 0.27 (=31.99 − 31.72) db image quality improvement

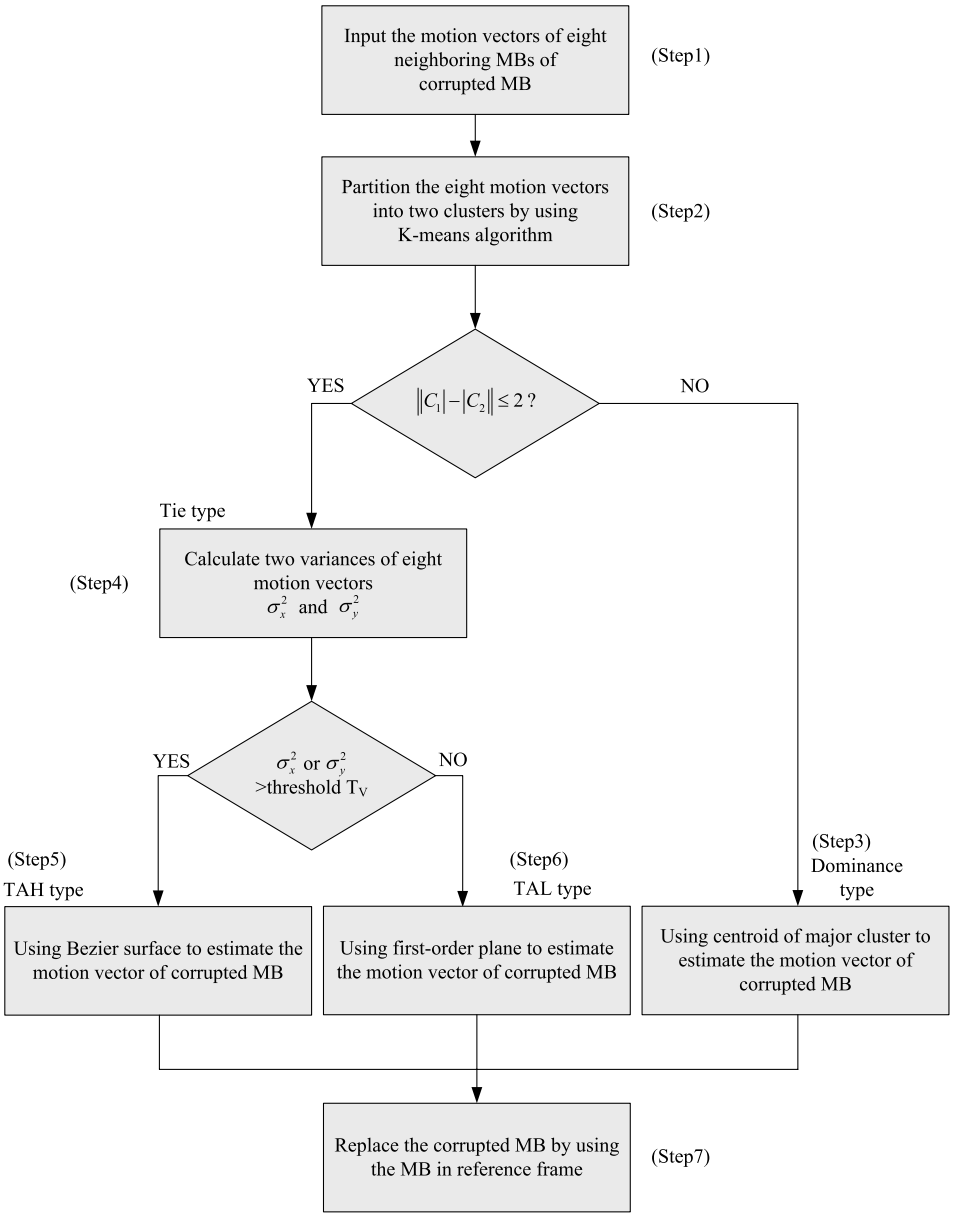

Fig. 7. Flowchart for the first seven steps in the proposed HEC algorithm.

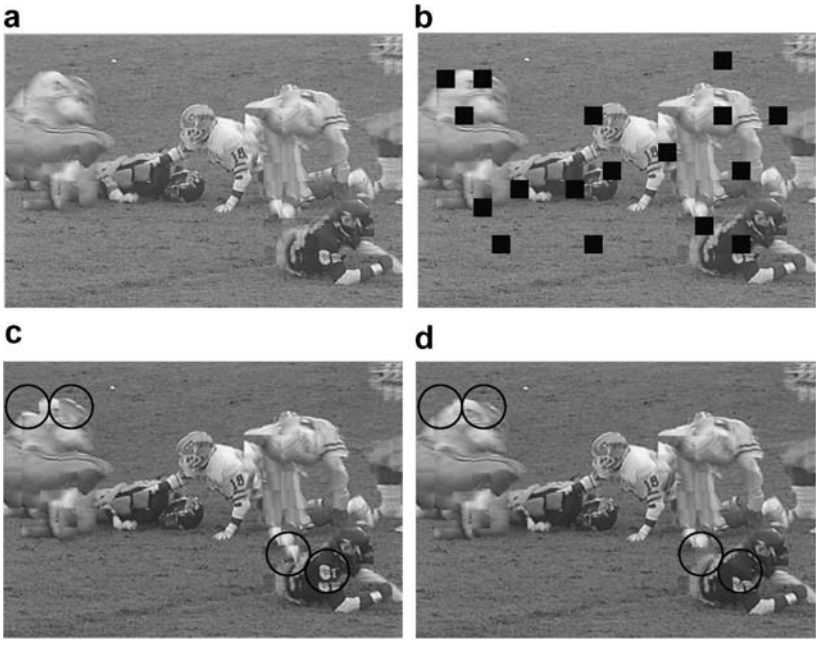

Fig. 8. The error-free and concealed image frames of the 11th frame in the Football sequence with 5% loss rate. (a) The error-free image frame. (b) The corrupted image frame. (c) The concealed image frame by using first-order plane estimation algorithm with 22.97 db. (d) The concealed result by using our proposed HEC algorithm with 23.48 db.

when compared to the first-order plane estimation algorithm.

Besides the image quality improvement (in terms of average PSNR) of our proposed HEC algorithm mentioned in the last paragraph, the visual quality improvement of our proposed algorithm is demonstrated in this paragraph and the next paragraph for the corrupted MBs being the dominance type and the TAH type, respectively.

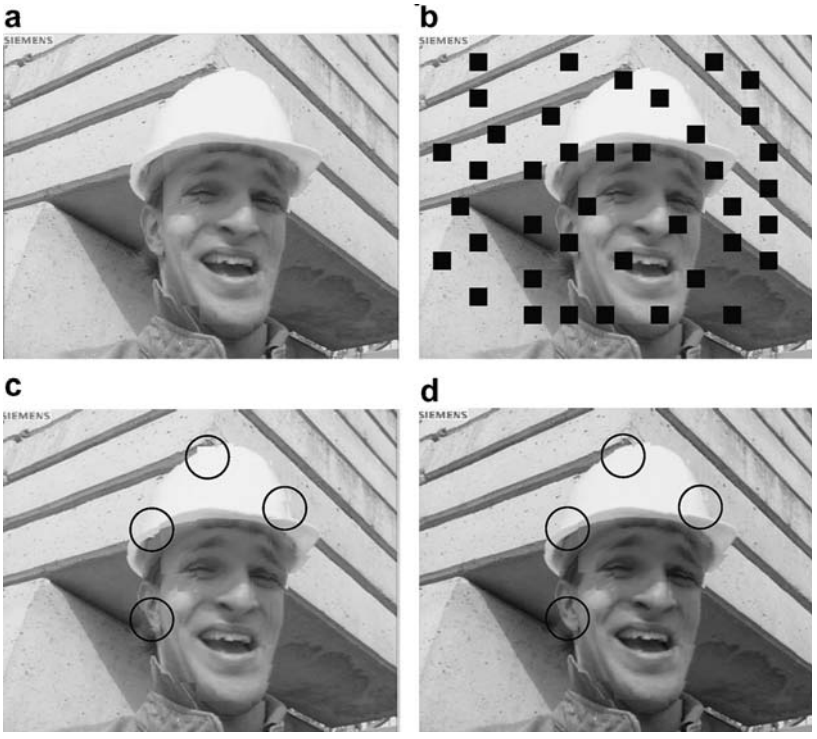

Fig. 9. The error-free and concealed image frames of the 16th frame in the Foreman sequence with 10% loss rate. (a) The error-free image frame. (b) The corrupted image frame. (c) The concealed image frame by using first-order plane estimation algorithm with 31.28 db. (d)The concealed result by using our proposed HEC algorithm with 31.68 db.

Table 1
Image quality comparison for six testing sequences with 5% loss rate

Sequences	Foreman	Stefan	Salesman	Akiyo	Mobile & Calendar	Football	Average PSNR
$PSNR_{EF}$	33.96	25.30	34.67	43.94	31.78	23.89	32.25
$PSNR_{FOP}$	33.43	25.08	34.23	43.66	31.48	23.42	31.88
$PSNR_{HEC}$	33.70	25.15	34.51	43.87	31.63	23.53	32.07

Table 2
Image quality comparison for six testing sequences with 10% loss rate

Sequences	Foreman	Stefan	Salesman	Akiyo	Mobile & Calendar	Football	Average PSNR
$PSNR_{EF}$	33.96	25.30	34.67	43.94	31.78	23.89	32.25
$PSNR_{FOP}$	32.88	24.87	33.87	43.46	31.23	23.00	31.55
$PSNR_{HEC}$	33.48	25.02	34.35	43.80	31.54	23.22	31.9

Table 3
Average frame execution time comparison for six testing sequences with 10% loss rate

Sequences	Foreman	Stefan	Salesman	Akiyo	Mobile & calendar	Football	Average time
$TIME_{FOP}$(s)	0.0703	0.0647	0.0694	0.0629	0.0579	0.0596	0.0641
$TIME_{HEC}$(s)	0.0687	0.0692	0.0632	0.0532	0.0594	0.0603	0.0624

Fig. 8a illustrates the original 11th error-free image frame in the Football video sequence. Under 5% loss rate for Fig. 8a, Fig. 8b depicts the corrupted image where the randomly selected corrupted MBs are denoted by black boxes. Fig. 8c demonstrates four concealed MBs by using the first-order plane estimation and Fig. 8d demonstrates the corresponding four concealed MBs by using our proposed HEC algorithm. It is observed that our proposed HEC algorithm has better visual effect (see the parts inside the four circles). In Fig. 8c and d, all the four corrupted MBs inside the four circles are of dominance type. When the corrupted MB is of dominance type, instead of using the first-order plane estimation, using the centroid of major cluster estimation to conceal the corrupted MB can have better visual effect since it is highly possible that the corrupted MB is a portion of the major cluster.

In this paragraph, the visual quality improvement of our proposed algorithm is demonstrated again. Fig. 9a illustrates the 16th error-free image frame in the Foreman video sequence. Under 10% loss rate for Fig. 9a, Fig. 9b depicts the corrupted image where the randomly selected corrupted MBs are denoted by black boxes. Fig. 9c demonstrates four concealed MBs by using the first-order plane estimation and Fig. 9d demonstrates the corresponding four concealed MBs by using our proposed HEC algorithm. It is observed that our proposed HEC algorithm has better visual effect (see the parts inside the four circles). In Fig. 9c and d, the top corrupted MB inside the top circle is of dominance type and the remaining three corrupted MBs are of TAH type. When the corrupted MB is of TAH (dominance) type, using the Bézier surface (centroid of major cluster) estimation to conceal the corrupted MB can have better visual effect. The readers can compare the four concealed MBs with the ones in Fig. 9a.

Finally, based on the above same testing video sequences, Table 3 is used to demonstrate the execution time comparison between the previous first-order plane estimation algorithm and our proposed HEC algorithm. From the average execution time comparison in Table 3, it is observed that under the same loss rate, our proposed HEC algorithm has little better execution-time performance.

5. Conclusions

The proposed HEC algorithm for error concealment has been presented in this paper. Based on neighboring MBs of the corrupted MBs, the corrupted MBs can be classified into three types by using our proposed novel adaptive estimation scheme. According to the classified type of the current corrupted MB, our proposed hybrid error concealment algorithm can determine what kind of error concealment method should be used to achieve better image quality and execution-time performance. Experimental results demonstrate that our proposed hybrid error concealment algorithm can improve the video quality and the execution-time performance over different loss rates.

References

[1] M. Al-Mualla, N. Canagarajah, D.R. Bull, Temporal error concealment using motion field interpolation, Electron. Lett. 35 (1999) 215–217.
[2] M.J. Chen, L.G. Chen, R.M. Weng, Error concealment of lost motion vectors with overlapped motion compensation, IEEE Trans. Circuits Syst. Video Technol. 7 (1997) 560–563.
[3] M.J. Chen, C.S. Chen, M.C. Chi, Temporal error concealment algorithm by recursive block–matching principle, IEEE Trans. Circuits Syst. Video Technol. 15 (2005) 1385–1393.
[4] W.J. Chu, J.J. Leou, Detection and concealment of transmission errors in H. 261 images, IEEE Trans. Circuits Syst. Video Technol. 8 (1998) 74–84.

[5] J. Feng, K. Lo, H. Mehropour, A.E. Karbowiak, Error concealment for MPEG video transmissions, IEEE Trans. Consumer Electron. 43 (1997) 183–187.
[6] J.D. Foley, A. van Dam, S.K. Feiner, J.F. Hughes, Computer Graphics: Principles and Practice Section 11.1.1.3: Plane Equations, second ed., Addison Wesley, New Jersey, 1996.
[7] D. Hearn, M.P. Baker, Computer Graphics, Section 10.8: Bézier Curves and Surfaces, second ed., Prentice Hall, New Jersey, 2002.
[8] S.K. Jang, J.B. Ra, Efficient error localization and temporal concealment based on motion estimation of enlarged block, J. Vis. Commun. Image Representation 14 (2003) 526–542.
[9] K.W. Kang, S.H. Lee, T. Kim, Recovery of coded video sequences from channel errors, Proc. SPIE. 2501 (1995) 19–27.
[10] L.W. Kang, J.J. Leou, A hybrid error concealment scheme for MPEG-2 video transmission based on best neighborhood matching algorithm, J. Vis. Commun. Image Representation 16 (2005) 288–310.
[11] C.S. Kim, R.C. Kim, S.U. Lee, An error detection and recovery algorithm for compressed video signal using source level redundancy, IEEE Trans. Image Process. 9 (2000) 209–219.
[12] Y.C. Lee, Y. Altunbasak, R. Mersereau, A temporal error concealment method for MPEG coded video using a multi-frame boundary matching algorithm, in: Proc. IEEE Int. Conf. Image Process., vol. 1, Oct. 2001, pp. 990–993.
[13] J.W. Park, S.U. Lee, Recovery of corrupted image data based on the NURBS interpolation, IEEE Trans. Circuits Syst. Video Technol. 9 (1999) 1003–1008.
[14] H.C. Shyu, J.J. Leou, Detection and concealment of transmission errors in MPEG-2 images—genetic algorithm approach, IEEE Trans. Circuits Syst. Video Technol. 9 (1999) 937–948.
[15] G.J. Sullivan, T. Wiegand, T. Stockhammer, Using the draft H.26 L video coding standard for mobile application, in: Proc. IEEE Int. Conf. Image Process., vol. 3, Oct. 2001, pp. 573–576.
[16] S. Tsekeridou, I. Pitas, MPEG-2 error concealment based on blockmatching principles, IEEE Trans. Circuits Syst. Video Technol. 10 (2000) 646–658.
[17] Z. Wang, Y. Yu, D. Zhang, Best neighborhood matching: an information loss restoration technique for block-based image coding systems, IEEE Trans. Image Process. 7 (1998) 1056–1061.
[18] W. Zeng, B. Liu, Geometric-structure-based error concealment with novel applications in block-based low-bit-rate coding, IEEE Trans. Circuits Syst. Video Technol. 9 (1999) 648–665.
[19] J. Zhang, J.F. Arnold, M.R. Frater, A cell-loss concealment technique for MPEG-2 coded video, IEEE Trans. Circuits Syst. Video Technol. 10 (2000) 659–665.
[20] Y. Zhao, M.M. Hannuksela, D. Tian, M. Gabbouj, Spatial error concealment based on directional decision and intra prediction, in: Proc. IEEE Int. Symp. Circuits and Syst., May 2005, pp. 2899–2902.
[21] J. Zheng, L.P. Chau, Error-concealment algorithm for H.26 L using first-order plane estimation, IEEE Trans. Multimedia 6 (2004) 801–805.
[22] Q.F. Zhu, Y. Wang, L. Shaw, Coding and cell-loss recovery in DCT-based packet video, IEEE Trans. Circuits Syst. Video Technol. 3 (1993) 248–258.